Reduction of FWM noise in WDM-based QKD systems using interleaved and unequally spaced channels

Yongmei Sun (孙咏梅)*, Yishan Lu (卢奕杉), Jianing Niu (牛佳宁), and Yuefeng Ji (纪越峰)

State Key Laboratory of Information Photonics and Optical Communications, Beijing University of Posts and Telecommunications (BUPT), Beijing 100876, China

**Corresponding author: ymsun@bupt.edu.cn*

Received December 8, 2015; accepted March 4, 2016; posted online May 10, 2016

To extensively deploy quantum key distribution (QKD) systems, copropagating with classical channels on the same fiber using wavelength division multiplexing (WDM) technology becomes a critical issue. We propose a user-based channel-interleaving WDM scheme with unequal frequency spacing (UFS-iWDM) to reduce the impairment on the quantum channels induced by four-wave mixing (FWM), and theoretically analyze its impact on quantum bit error rate (QBER). Numerical simulation results show that a UFS-iWDM can significantly reduce the FWM noise and improve QBER compared with the corresponding WDM scheme with equal frequency spacing (EFS), especially in the case of nonzero dispersion shifted fiber.

OCIS codes: 270.5565, 060.2330, 060.4510.
doi: 10.3788/COL201614.060602.

Quantum key distribution (QKD)[1] is considered as a promising technology for information security. In the past years, great progress has been achieved on single-photon-based point-to-point optical fiber QKD system. In such QKD systems, quantum signals are mostly transmitted through dedicated fibers to keep the ultra-weak quantum signals from the impact of the classical optical signals. However, it is extremely expensive and impractical for extensive deployment. To make QKD more practicable, it should be compatible with classical optical networks using wavelength division multiplexing (WDM) technique. Therefore, the next step is to be integrated with existing WDM systems[2]. Xia *et al.*[3] firstly reported simultaneous QKD and high-speed data communications over the installed fiber. More recent works have realized QKD with copropagating a few classical channels[4–8]. However, they have not considered the impact of four-wave mixing (FWM).

Generally, copropagating with classical channels severely impair quantum channels whose powers are ultra-low[9]. The impairment sources include Raman scattering, channel crosstalk, and FWM[10,11]. Several solutions proposed to reduce such impairments are as follows. (1) To reduce the effect of Raman scattering, the quantum channels were usually placed at the higher frequency channels and enough frequency spacing remained between quantum and classical channels[12,13]. (2) Channel crosstalk was reduced by increasing the isolation between the WDM channels[10,14]. (3) The impairment of FWM can be mitigated by reducing the classical channel power, increasing the spacing between channels, and using orthogonal polarization on quantum and classical channel, respectively[14,15].

In future WDM-based QKD systems supporting multiple users, quantum signals will face up to more complicated environment since each user generally needs three channels (wavelengths) to transmit three type of signals, i.e., quantum signal, synchronization signal for detecting quantum signal at the receiver, and data signal with different power levels, respectively, which will be multiplexed in one fiber. Other situations also include multiplexing the synchronization and data channels in one fiber[16], and time-division-multiplexing quantum and data signals on one channel[17]. Multiplexing multiple users' channels in a single fiber will give rise to more serious impairments. The impairments induced by Raman scattering and crosstalk can be efficiently reduced by placing quantum channels on the higher frequencies and using high-isolation filters, respectively. However, it is difficult to eliminate FWM noise by using the approaches mentioned above. Furthermore, FWM will be the dominant impairment in low-dispersion fibers[14].

To solve this problem, we proposes a user-based channel-interleaving WDM scheme with unequal frequency spacing (UFS-iWDM) to reduce the impairment induced by FWM, and theoretically analyze its impact on the quantum bit error rate (QBER). Numerical simulation results show that UFS-iWDM can significantly reduce the FWM noise and improve QBER compared with the corresponding WDM scheme with equal frequency spacing (EFS).

FWM is a nonlinearity effect that occurs due to the interaction between three optical channels through the third-order electric susceptibility of the optical fiber. Assuming there are three optical channels at frequencies f_i, f_j and f_k $(k \neq i, j)$ separately, they will mix to generate a new wave of frequency

$$f_{ijk} = f_i + f_j - f_k. \tag{1}$$

The peak power of the mixing product is given by Refs. [14,18] using the equations

$$P_{ijk} = \frac{\eta D^2 \gamma^2 P_i P_j P_k e^{-\alpha z}}{9\alpha^2}[1 - e^{-\alpha z}]^2, \quad (2)$$

$$\eta = \frac{\alpha^2}{\alpha^2 + \Delta\beta^2}\left\{1 + \frac{4e^{-\alpha z}\sin^2\left(\frac{\Delta\beta Z}{2}\right)}{[1 - e^{-\alpha z}]^2}\right\}, \quad (3)$$

$$\Delta\beta = \beta_{ijk} + \beta_k - \beta_i - \beta_j, \quad (4)$$

where P_i, P_j, and P_k denotes the power of the three original channels, respectively, η denotes the FWM efficiency, α denotes the attenuation coefficient of the fiber, z denotes the fiber length, γ denotes the fiber nonlinearity coefficient, D denotes the FWM degeneracy factor, $\Delta\beta$ denotes the phase-matching factor, and β denotes the phase constant. For three channels at different frequencies (non-degenerate case), $D = 6$. For two channels (degenerate case, $I = j$, $f_i = f_j$), $D = 3$.

Figure 1 shows a WDM-based QKD system architecture supporting multiple users, which is typical for end-to-end metropolitan applications. At the transmitter, QKD TX, SYN, and Data modules generate quantum, synchronization, and data signals, respectively. At the receiver, QKD RX, SYN, and Data modules receive the corresponding signals, respectively. DWDM is used to multiplex or demultiplex multiple channels; FM, PM and BS form an interference ring; VOA, NBF and SPD are used to adjust attenuation, isolate noises, and detect photons respectively. For any end-to-end users to realize QKD and encrypted data communication, there are many orders of magnitude differences among power levels of quantum, synchronization, and data signal, e.g., −82, −10, and 0 dBm, respectively. Obviously, severe noise power that falls at a quantum channel will ultimately worsen QBER. Therefore, we propose a UFS-iWDM scheme to reduce the impairment, and analyze its impact on the QBER.

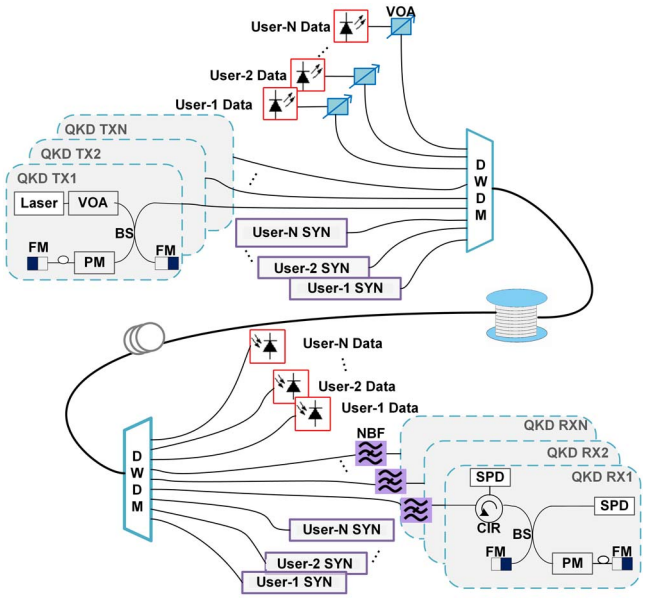

Fig. 1. WDM-based QKD system architecture. VOA: variable optical attenuator; BS: beam splitter; FM: Faraday mirror; PM: phase modulator; and NBF: narrow band filter.

The basic idea of the UFS-iWDM scheme is shown in Fig. 2; it has two features: (1) three channels of each user are interleaved, and all quantum, synchronization, and data channels are, respectively, arranged to the higher, middle, and lower frequencies, which can efficiently reduce the impacts of Raman scattering and crosstalk; (2) UFS is exploited to reduce the FWM noise. If the frequency spacing of any two channels is different from that of other, no FWM power will fall at the assigned channels[19]. Therefore, the key issue of UFS-iWDM is to find out the optimal frequency spacings, which can be simplified to an NP-complete integer linear programming (ILP) problem[19]. To get an approximate solution, the available frequency bandwidth is first divided into equal blocks with bandwidth Δf. Then all frequency spacings for N users, which is denoted as $n_i\Delta f$ (n_i is an integer and $i = 1, 2, ..., 3N - 1$), will be found. During this procedure, $3N(3N-1)/2$ partial sums of adjacent n_i should be different from each other, and the total sum of n_i should be minimized. Note that UFS-iWDM can find more than one set of $n_i\Delta f$ that removes FWM noises on all assigned channels. Since there are big differences among the power levels of three type of signals, the set of $n_i\Delta f$ with the largest frequency spacing between adjacent quantum and synchronization channels is selected to be the best one, thus other noise that falls at the quantum channel will be the lowest. However, it means that the UFS-iWDM will spend more time to find all sets of $n_i\Delta f$ and select the best one. In a word, due to the ultra-low powers of quantum channels, the large differences between UFS-iWDM and the classical UFS approach are: (1) interleaving all users' channels and placing all quantum channels on the higher frequencies before calculating n_i; (2) finding the best solution after calculating n_i.

To evaluate the performance of the UFS-iWDM, we need to derive a QBER formula. The QBER is defined as the number of erroneously detected photons over the total number of detected photons. Without considering

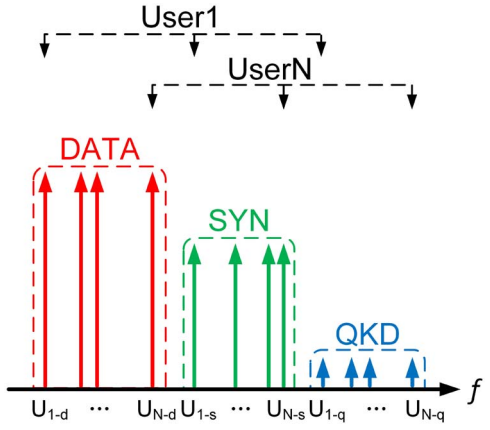

Fig. 2. Channel allocation in the UFS-iWDM scheme.

Raman scattering and after-pulse, the errors come from the nonideal interference visibility of the QKD components, dark counts of single-photon detector (SPD), and the noise induced by channel crosstalk and FWM. Referring to the analysis approach in Refs. [10,20], we derive the QBER of a pair of end-to-end users in a WDM-based QKD system. Assuming that the most popular BB84 protocol[1] is adopted and two SPDs are used in the receiver, the derived QBER is

$$\mathrm{QBER} = \frac{\frac{1-V}{2} R_{\mathrm{sift}} + \frac{1}{2}(R_{dc} + R_{ct} + R_{\mathrm{FWM}})}{R_{\mathrm{sift}} + R_{dc} + (R_{ct} + R_{\mathrm{FWM}})}, \quad (5)$$

where V denotes the interference visibility; R_{sift} denotes the quantum key rate after sifting between end-to-end users; and R_{dc}, R_{ct}, and R_{FWM} denote the number of detected photons per second due to dark counts, channel crosstalk, and FWM noise, respectively, 50% of which will be erroneously detected from the viewpoint of probability.

Considering the QKD system which adopts a Faraday-Michelson interferometer (FMI)[21] to realize BB84 protocol, we derive the formulae

$$R_{\mathrm{sift}} = q\delta f_{\mathrm{rep}} \mu \eta_{\mathrm{spd}} \times 10^{-0.1(\alpha z + A_0 + A_d)}, \quad (6)$$

$$R_{dc} = 2 q f_{\mathrm{rep}} P_{\mathrm{dark}}, \quad (7)$$

$$R_{ct} = q\delta \frac{P_{ct}\lambda}{hc} f_{\mathrm{rep}} \Delta\tau_{\mathrm{gate}} \eta_{\mathrm{spd}} \times 10^{-0.1(\alpha z + A_0 + I_s)}, \quad (8)$$

$$R_{\mathrm{FWM}} = q\delta \frac{P_{\mathrm{FWM}}\lambda}{hc} f_{\mathrm{rep}} \Delta\tau_{\mathrm{gate}} \eta_{\mathrm{spd}} \times 10^{-0.1(A_0 + A_d)}, \quad (9)$$

where $q = 0.5$ denotes the efficiency of BB84 protocol, $\delta = 0.5$ denotes the FMI-related loss, f_{rep} denotes the pulse repetition rate of quantum signal, μ denotes the mean number of photons per pulse, η_{spd} denotes the SPD efficiency, P_{dark} denotes the probability of the dark counts occurring in one of the SPDs during each detection, P_{ct} and P_{FWM} denotes the crosstalk and FWM power that fall at the quantum channel, respectively, λ denotes wavelength, h denotes Planck constant, c denotes the light speed, $\Delta\tau_{\mathrm{gate}}$ denotes the gate duration of SPD, α denotes the attenuation coefficient, z denotes the fiber length, A_0 and A_d denote the insert loss of fiber connector and MUX/DEMUX, respectively, and I_s denotes the isolation degree induced by NBF and DEMUX.

To evaluate the performance of the UFS-iWDM, we define the corresponding WDM scheme with EFS named EFS-iWDM, to be a benchmark. Its difference from UFS-iWDM is that all frequency spacings are equal.

A simulation is run based on MATLAB. The main parameters are shown in Table 1, which reference typical values used in the literature and commercial devices. In Table 1, f_s denotes the frequency spacing; P_q, P_{syn}, and P_{data} denote the launched quantum, synchronization, and data signal power per channel, respectively.

The FWM power and QBER on a given quantum channel for UFS-iWDM and EFS-iWDM are simulated and compared under different system parameters, i.e., fiber length, fiber type, frequency spacing, and power level of signal. Here, two type of fibers widely used in the classical WDM system are selected, i.e., standard single mode fiber (SSMF) and non-zero dispersion shifted fiber (NZ-DSF).

Since the FWM power that falls at each quantum channel is zero in the UFS-iWDM scheme, only the EFS-iWDM is analyzed in Figs. 3–5 to show the impact of FWM noise. As shown in Figs. 3 and 4, where $N = 4$, the FWM power decreases with the increase of the fiber length and the frequency spacing, and it becomes more than 15 dB obviously lower when P_{syn} decreases from 0 to −10 dBm because the synchronization channel is assigned closer to the quantum channel. For NZ-DSF, the FWM power is nearly 20 dB higher than that of SSMF as shown in Fig. 4, since the phase-matching condition can be met more easily for a smaller dispersion in NZ-DSF.

The effect of the number of users (N) is shown in Fig. 5, where $z = 25$ km. We observe that the FWM power increases with the increase of N when $P_{\mathrm{syn}} = 0$ dBm, while it does not hold when $P_{\mathrm{syn}} = -10$ dBm. The reason is that the powerful data channel with 0 dBm becomes farther from the quantum channel with the increase of N in Fig. 5(b).

Because the launched quantum signal is only −82 dBm, the FWM noise has a significant impact on the quantum signal, especially in the case of NZ-DSF or narrower frequency spacing or higher classical signal power in the EFS-iWDM scheme, as analyzed above. However, there is no FWM noise on any assigned channels in the UFS-iWDM scheme using the UFS listed in Table 2 where

Table 1. Main Parameters Used in the Simulation

Parameter	Value
f_s	50–1000 GHz
z	0–25 km
P_q	−82 dBm
P_{syn}	0.1–2 mW
P_{data}	0 dBm
N	1–4
f_{rep}	500 MHz
μ	0.1
V	97%
P_{dark}	5×10^{-8}
η_{spd}	11%
α	0.2 dB/km
A_0	1.5 dB
A_d	5 dB
I_s	80–105 dB
Δt_{gate}	500 ps

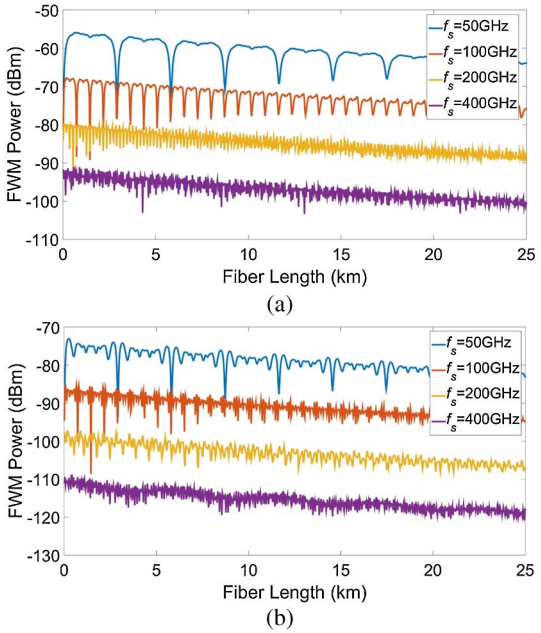

Fig. 3. FWM power versus fiber length in the EFS-iWDM; (a) $P_{\text{syn}} = 0$ dBm and (b) $P_{\text{syn}} = -10$ dBm.

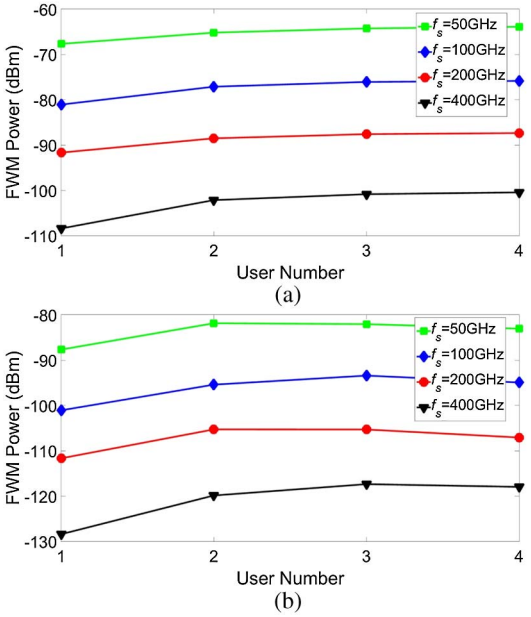

Fig. 5. FWM power versus number of users in the EFS-iWDM; (a) $P_{\text{syn}} = 0$ dBm and (b) $P_{\text{syn}} = -10$ dBm.

BW denotes the whole bandwidth. For fair comparison, the whole bandwidths assigned to the UFS-iWDM and the EFS-iWDM are set to be the same in the simulations.

Next, the QBER of a given quantum channel is simulated for the UFS-iWDM and the EFS-iWDM. In Figs. 6 and 7, where $N = 4$ and $z = 25$ km, the dot line means the QBER = 11% which is the maximum value to ensure normal QKD operation. For simplifying the expression, average frequency spacing is used in Fig. 6(b). As shown in Fig. 6, the QBER of the UFS-iWDM outperforms the EFS-iWDM, especially when the frequency spacing is narrower than 400 GHz. We also observe that the QBER increases to nearly 7% when the average frequency spacing is 100 GHz in the UFS-iWDM; the reason is that cross talk becomes very high although FWM noise is zero.

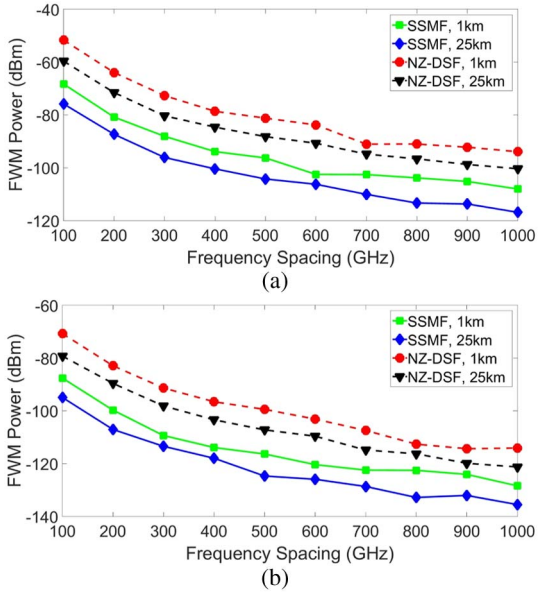

Fig. 4. FWM power versus frequency spacing in the EFS-iWDM; (a) $P_{\text{syn}} = 0$ dBm and (b) $P_{\text{syn}} = -10$ dBm.

In Fig. 7, where $f_s = 200$ GHz, the UFS-iWDM greatly outperforms the EFS-iWDM, especially in NZ-DSF. For the UFS-iWDM, the QBER is far from 11% when $P_{\text{syn}} < 2$ mW, while the EFS-iWDM could not ensure normal QKD operation when $P_{\text{syn}} > 1$ mW SSMF, or when $P_{\text{syn}} > 0.2$ mW NZ-SMF. Furthermore, Figs. 6 and 7 also show that the UFS-iWDM works well on both SSMF and NZ-DSF.

In real-life QKD systems, coherent light sources attenuated to single-photon levels are widely employed with decoy state modulation. Thus, the typical secure up bound of the QBER may be 5%–8%. In this stricter case, the UFS-iWDM also works well and outperforms the EFS-iWDM, as shown in Figs. 6 and 7.

It should be noted that, for simplicity, we ignore the effect of data modulation format. If taking the randomness of bit sequences into account, the degenerate FWM model we cited is practicable in the case of non-return-to-zero (NRZ), no walkoff, and no initial delay between interacting channels[22,23]. Here the walkoff can be

Table 2. Frequency Spacing Assigned in UFS-iWDM

N	$f_s = n_i \Delta f$ in UFS-iWDM
1	$n_i = 1$, 2, and $\Delta f = \text{BW}/3$
2	$n_i = 3$, 4, 5, 6, 2, and $\Delta f = \text{BW}/20$
3	$n_i = 9$, 8, 4, 10, 5, 11, 7, 6, and $\Delta f = \text{BW}/60$
4	$n_i = 9$, 13, 6, 10, 14, 7, 11, 15, 8, 12, 5, and $\Delta f = \text{BW}/110$

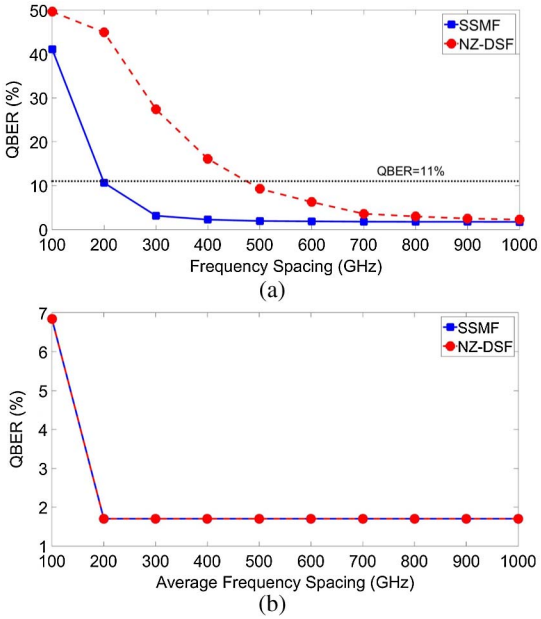

Fig. 6. QBER versus frequency spacing; (a) the EFS-iWDM and (b) the UFS-iWDM.

ignored because its effect is small in the case of NRZ[23,24]. In the situation of using other modulation and coding formats, the randomness of bit sequences should be considered to obtain exact FWM model by referring to the methods presented in Refs. [23–25]. In addition, the QKD system we analyzed is a typical example for metropolitan applications where complex components, like switcher and repeater, are not necessary. In the future, we will analyze more complex QKD system for wide area network applications.

In conclusion, we propose a UFS-iWDM scheme to reduce the impairment induced by FWM, and theoretically derive its impact on the QBER. Numerical simulation results show that the UFS-iWDM can avoid FWM noise in any case of different fiber length, fiber type, frequency spacing, and signal power, compared with the EFS-iWDM. The QBER of the UFS-iWDM outperforms that of the EFS-iWDM especially in the case of less than 400 GHz of frequency spacing or higher than 0.6 mW of classical signal power for SSMF, or any case for NZ-DSF.

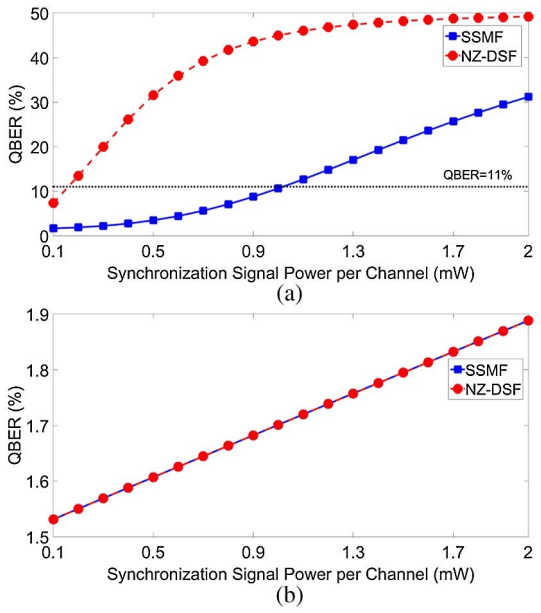

Fig. 7. QBER versus synchronization signal power per channel; (a) the EFS-iWDM and (b) the UFS-iWDM.

This work was supported by the National Natural Science Foundation of China under Grant No. 61331008.

References

1. C. H. Bennett and G. Brassard, in *Proceedings of the IEEE International Conference on Computers, Systems and Signal Processing*, 175 (1984).
2. H. Rohde, S. Smolorz, A. Poppe, and H. Huebel, in *Proceedings of OFC/NFOEC 2008*, OTuP1 (2008).
3. T. Xia, D. Chen, G. A. Wellbrock, A. Zavriyev, A. C. Beal, and K. M. Lee, in *Proceedings of OFC/NFOEC 2006*, OTuJ7 (2006).
4. K. A. Patel, J. F. Dynes, M. Lucamarini, I. Choi, A. W. Sharpe, Z. L. Yuan, R. V. Penty, and A. J. Sheilds, Appl. Phys. Lett. **104**, 051123 (2014).
5. I. Choi, Y. R. Zhou, J. F. Dynes, Z. Yuan, A. Klar, A. Sharpe, A. Plews, M. Lucamarini, C. Radig, J. Neubert, H. Griesser, M. Eiselt, C. Chunnilall, G. Lepert, A. Sinclair, J. Elbers, A. Lord, and A. Sheilds, Opt. Express **22**, 23121 (2014).
6. A. Ciurana, J. Martinez-Mateo, M. Peev, A. Poppe, N. Walenta, H. Zbinden, and V. Martín, Opt. Express **22**, 1576 (2014).
7. S. Wang, W. Chen, Z. Yin, H. Li, D. He, Y. Li, Z. Zhou, X. Song, F. Li, D. Wang, H. Chen, Y. Han, J. Huang, J. Guo, P. Hao, M. Li, C. Zhang, D. Liu, W. Liang, C. Miao, P. Wu, G. Guo, and Z. Han, Opt. Express **22**, 21739 (2014).
8. L. Wang, L. Chen, L. Ju, M. Xu, Y. Zhao, K. Chen, Z. Chen, T. Chen, and J. Pan, Appl. Phys. Lett. **106**, 081108 (2015).
9. S. Aleksic, D. Winkler, A. Poppe, G. Franzl, B. Schrenk, and F. Hipp, in *Proceedings of 15th International Conference on Transparent Optical Networks*, 1 (2013).
10. P. Eraerds, N. Walenta, M. Legré, N. Gisin, and H. Zbinden, New J. Phys. **12**, 063027 (2010).
11. N. Yu, Z. Dong, J. Wang, Z. Wei, and Z. Zhang, Chin. Opt. Lett. **12**, 102703 (2014).
12. P. Toliver, R. J. Runser, T. E. Chapuran, S. McNown, M. S. Goodman, J. Jacket, R. J. Hughes, C. G. Peterson, K. McCabe, J. E. Nordholt, K. Tyagi, P. Hiskett, and N. Dallman, in *Proceedings of the 17th Annual Meeting of the IEEE*, 491 (2004).
13. H. Kawahara, A. Medhipour, and K. Inoue, Opt. Commun. **284**, 691 (2011).
14. N. A. Peters, P. Toliver, T. E. Chapuran, R. J. Runser, S. R. McNown, C. G. Peterson, D. Rosenberg, N. Dallmann, R. J. Hughes, K. P. McCabe, J. E. Nordholt, and K. T. Tyagi, New J. Phys. **11**, 045012 (2009).
15. N. A. Peters, P. Toliver, T. E. Chapuran, R. J. Runser, S. R. McNown, C. G. Peterson, D. Rosenberg, N. Dallmann, R. J. Hughes, K. P. McCabe, J. E. Nordholt, and K. T. Tyagi, in *Proceedings of OFC/NFOEC 2010*, OTuKl (2010).
16. X. M. Lu, L. J. Zhang, Y. G. Wang, W. Chen, D. J. Huang, D. Li, S. Wang, D. Y. He, Z. Q. Yin, Y. Zhou, C. Hui, and Z. F. Han, Sci. China Phys. Mech. Astron. **58**, 120301 (2015).

17. X. F. Mo, I. Lucio-Martinez, P. Chan, C. Healey, S. Hosier, and W. Tittel, Opt. Express **19**, 17729 (2011).
18. F. Forghieri, R. W. Tkach, and A. R. Chraplyvy, *Optical Fiber Telecommunications* (Elsevier, 1997).
19. F. Forghieri, R. W. Tkach, A. R. Chraplyvy, and D. Marcuse, IEEE Photon. Technol. Lett. **6**, 754 (1994).
20. P. D. Kumavor, A. C. Beal, S. Yelin, E. Donkor, and B. C. Wang, IEEE J. Lightwave Technol. **23**, 268 (2005).
21. X. Song, H. Li, C. Zhang, D. Wang, S. Wang, Z. Yin, W. Chen, and Z. Han, Chin. Opt. Lett. **13**, 012701 (2015).
22. S. Song, C. Allen, K. Demarest, L. Pelz, X. Fang, and Y. Pua, in *Proceedings of LEOS '97*, Vol. **2**, 224 (1997).
23. S. Kumar, IEEE J. Lightwave Technol. **23**, 310 (2005).
24. A. Akhtar, L. Pavel, and S. Kumar, IEEE J. Lightwave Technol. **24**, 4269 (2006).
25. J. X. Du, Opt. Commun. **282**, 2983 (2009).